Artificial neural network for the prediction of the fresh properties of cementitious materials

Malo Charrier, Claudiane M. Ouellet-Plamondon *

École de Technologie Supérieure, Université du Québec, Montreal, Quebec H3C 1K3, Canada

ARTICLE INFO

ABSTRACT

The admixtures influence the fresh properties of cement paste, which is a key factor in the ink design for 3D printing applications. In this study, the mix contained superplasticizer and four other admixtures (calcium silicate hydrate seeds, nanoclay, viscosity-modifying agent, accelerator) based on a factorial experimental design plan. The cement paste yield stresses measured with the rheometer are compared with the mini-slump test. An empirical relationship is proposed between the dynamic yield stress and the mini-slump. The critical yield stress for printing one layer is calculated to ensure the material to maintain its shape under his own weight. Artificial Neural Networks (ANN) are trained to predict the mini-slump and the dynamic yield stress from specific admixture proportions of the mixture. The ANN defines the amount of each admixture based on the critical yield stress. Finally, the neural networks are validated through the simulation of new mixes and by a comparison of the yield stress and mini-slump from the simulation and from experiments.

1. Introduction

Three-dimensional printing for cementitious materials has a great potential to reduce cost of the construction industry and pave the way to innovation [1–3]. Nevertheless, there are still barriers to a wider use of these techniques. Generally, the concrete is pumped then extruded through a nozzle. The challenges start with the pumpability of the mix and the capacity of the printed layers to sustain their shape. The mastery of formulation in order to obtain the perfect consistency of the paste is one of the fundamental issues of 3D printed concrete. The main characteristic to assess a printable ink is the yield stress. Several methods are suitable to measure the yield stress such as the slump test or the use of a rheometer [4–12]. The yield stress measured here corresponds to the dynamic yield stress [13], we consider that it is the critical stress the material can withstand at the exit of the nozzle, that is to say after having been sheared, before flowing. To be able to control the yield stress and the other characteristics of the material, such as viscosity and cement hydration, admixtures are widely used. However, carrying out test campaigns to come up with the best printable ink can be experimentally demanding. To tackle the difficulty of designing a mix meeting the needs of 3D printing, some authors have focused on the science of machine learning and artificial neural networks (ANN) [14,15]. With this exploratory method, it is possible to obtain crucial information on

how the mixture will behave during and after printing, simply from its composition [16,17].

The objective of this study is to investigate the influence of several admixtures on the rheological properties of a printing mortar. Superplasticizers (SP) are often used in high-performance concrete since they are used to reducing the water content [18]. The most widely used SP is polycarboxylate; this polymer is adsorbed on cement particles, and then repulses other particles through the steric effect [19–21]. The use of a viscosity-modifying agent (VMA) increases the plastic viscosity at rest due to their interspersed polymers chains. Moreover, the flocculation capacity of the admixtures depends mostly on their molecular weight: by being adsorbed on the surface of cement grains, they can bridge the grains into a more stable microstructure [18]. Shearing a mixture containing VMA restores its workability, which in turn ensures the cohesion of a printed cement-based material layer. Viscosity modifying agents are often used along with superplasticizers [22], while accelerators are used to hasten hydration [18]. In the context of additive manufacturing, a faster hardening of the cement-based material can improve the building rate. These admixtures are useful for accelerating the production of precast concrete plants [23]. The C-S-H seeds are inclusions of calcium silicate hydrate (C-S-H) in a polymer dispersion. These act as accelerator admixtures by enhancing nucleation: new nucleation sites are available in the capillary pore space favorizing the precipitation of hydration products as C-S-H, the main hydration product in cement

---

* Corresponding author.
  E-mail address: claudiane.ouellet-plamondon@etsmtl.ca (C.M. Ouellet-Plamondon).

Note: Low-resolution images were used to create this PDF. The original images will be used in the final composition.

paste. This results in an early hydration peak and a reduction of the induction period [24,25]. Researchers agree on the fact that CSH seeds can benefit from the kinetics of the paste for digital printing [14,26]. However, the fresh properties brought about by the addition of CSH is not reported in most studies. The selected accelerator is a multicomponent, non-chloride, accelerating and water-reducing admixture formulated to accelerate concrete setting time and increase early and ultimate strengths for hot to subfreezing ambient temperatures. It is a generic accelerator for ready mix concrete and its action is delayed due to transportation time. It is foreseen to improve the buildability. Nanoclays are mineral compounds known for their rheological properties, and have been shown to enhance shape stability and viscosity [18,27, 28]. This admixture appears in a colloidal dispersion forming a gel that enhances viscosity and cohesion, and have a shear thinning behavior. This latter property can be explained by the nanoclays' charged surfaces and irregular microstructures [27,29].

The focus is on the cement paste, which accounts for most of the characteristics of the mortar [30,31], when accelerators are added. The Fig. 1 shows the schematic of the study. The experimental steps started with the mini-slump tests conducted to study the spread of the mixtures. In addition, the dynamic yield stress and viscosity of the cement paste were measured according to the recommendations of the National Institute of Standards and Technology [10]. Slump tests were conducted on mortars to find the critical yield stress. Regression models were developed to link to other measured properties. Finally, an Artificial Neural Network (ANN) was trained and tested to predict the yield stress and mini-slump as a function of the percentage of each admixture.

2. Materials and methods

2.1. Material and admixture properties

Binary cement with silica fumes (GUb-8SF), with a specific gravity of 2.8, is used in this study. The water used is normal tap water. A superplasticizer (SP) is added to increase the workability of each mixture. The SP is classified as Type A water-reducing admixture and Type F water-reducing, high range admixture according to ASTM C494/C494M [32]. The accelerator (A) has no chloride, has a water reducer effect, and therefore, increases the workability. It is classified as Type C accelerating admixtures and Type E water-reducing and accelerating admixtures. Hence, the effect of this admixture is first an increase of workability during mixing, then decrease of the set time of the mix. The strength-enhancing admixture (X) is a CSH seed admixture known to improve early cement hydration and enhance workability. Due to its nature, CSH seeds increase the rate of development of early strength of the mix by providing nucleation sites for hydrates. The use of a set accelerator (A) and a hardening accelerator (X) is justified by the different timing of each admixture and also by the different mechanism involved (chemical reaction and addition of particles). Nanoclays (C) are used to increase the stability of the mix. The viscosity-modifying agent (VMA) improves the stability and it is classified as a Type S admixture. The formulated product contains less than 1% diutan gum and less than 0.2% [1,1′-Biphenyl]-2-ol. The solid content of the admixtures is determined according to ASTM C494 [32]. Results are presented in Supplementary Table S1.

2.2. Mixing procedure

In order to achieve a good dispersion of the admixtures in the paste, the mixing procedure was completed following ASTM C1738. The paste obtained with this standard is expected to have rheological properties analogous to a concrete without its aggregates [33,34]. A high shear mixer with a water-cooling system was selected to meet specifications. At first, the water and the admixtures were added to the mixer and the temperature was controlled at 23 °C ± 2 °C. Next, the cement was poured within 60 s. The mixer was turned on for 30 s at a speed of 10,000 rpm. The paste was allowed to rest for 150 s. Finally, the paste was mixed at 10,000 rpm for 30 s.

2.3. Mini-slump test

The mini-slump test consisted in filling a cone with freshly mixed cement paste and lifting it slowly to allow the paste to flow under its own weight. The cone was a smaller version of the Abrams cone used for slump tests, and was designed and 3D-printed with the following dimensions: inside top diameter, 19 mm; inside base diameter, 38 mm; height, 57 mm, based on the shape reported in other studies [6,8,35]. It was placed on an acrylic plate marked with 20×20 mm^2 squares to form a grid.

First, cement was pumped manually into a syringe from the mixer and poured into the mini-cone. At 2 min after the end of the mixing, the
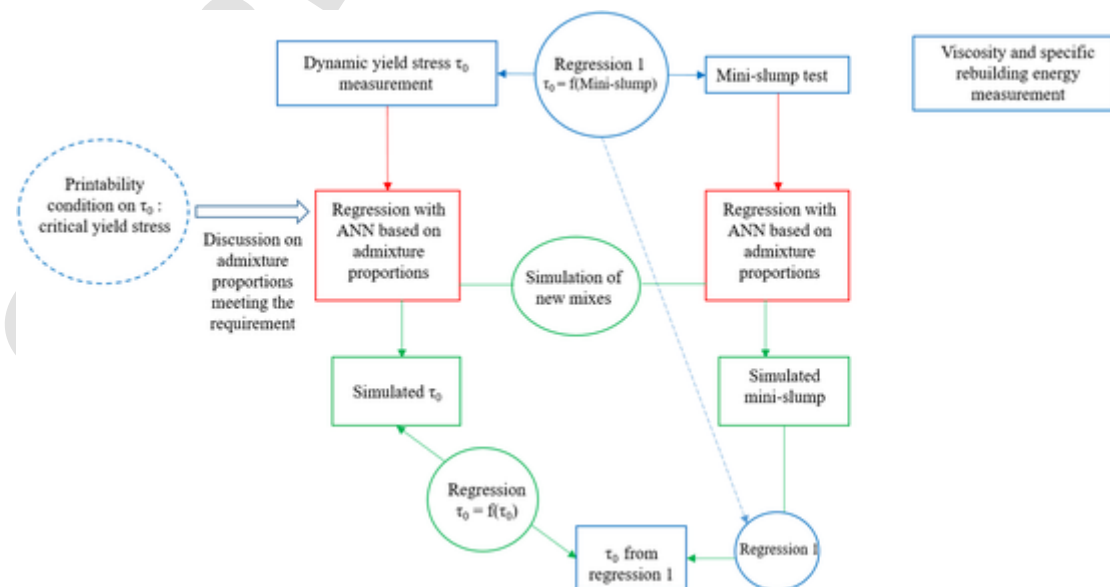

Fig. 1. Schematic representation of the study: in blue are the experimental measurement; in red the training of the neural network; and in green, the simulated results. (For interpretation of the references to colour in this figure legend, the reader is referred to the web version of this article.)

cone was removed and 5 s later, a photo was taken from the top of the set-up. While it is known that admixtures may take 15 min to be effective, the fresh properties were measured early on to simulate the behavior immediately after the accelerator was added. The four diameters were measured via ImageJ, an open source photo processing software application, using the grid for scale. The mini-slump spread S was computed as follows (inspired from the ASTMC1437 standard) [36]:

$$S = \frac{(mean\ of\ four\ diameters - inside\ base\ diameter)}{inside\ base\ diameter} \times 100 \qquad (1)$$

2.4. Rheological measurements

2.4.1. Calibration

Before measuring the rheological parameters of the paste, a calibration of the rheometer and the measuring tool was completed to ensure that they were operating properly. For this, the National Institute of Standards and Technology (NIST) proposes testing a calibrated paste, the Standard Reference Material (SRM) 2492 [37]. This mixture is composed of corn syrup, distilled water and limestone. Following the NIST recommendations, corn syrup is placed into a wide mouth plastic jar, and then distilled water is added. It is mixed by hand with a spatula for approximately 5 min or until the paste is homogenous. The mixture is poured into a high shear mixer, and the same mixing procedure is followed as for the cement paste to introduce limestone powder and mix [33].

The measuring tool was designed following the recommendations of the NIST. It is a 3D printed spindle with a geometry intended to decrease slippage [10]. The double spiral spindle is connected to the rheometer by a metal shaft (Fig. 2). This measuring tool has a diameter of 25 mm and is 55 mm long from the bottom to the top of the spiral.

The stainless-steel cup holder was filled with the SRM 2492 standard paste and placed into the rheometer using a controller to set the temperature at 23 °C ± 2 °C. Four tests were conducted, with the rotational speed controlled from 0.1 rpm to 100 rpm for 15 points (this is the up-curve), after which it was decreased from 100 rpm to 0.1 rpm (this is the down curve). While controlling the rotational speed, the torque was measured. The up-curve serves to reset the shear history of the paste. The average raw data of the down curves were computed and calibrated to fit the SRM 2492 certified values using the Bingham approach, as implemented in the SRM 2493 NIST certification [38]. Subsequently, the calibration factors K_τ and K_μ were identified from the NIST Data Calibration Tool, and were used to determine the shear rate, the shear stress, the yield stress and the viscosity when testing cement pastes.

2.4.2. Procedure to measure the dynamic yield stress of the cement pastes

The cement paste is tested 5 min after the mixing procedure. The test consists of an up-curve of 15 measurements from 0.1 rpm to 100 rpm and a down curve of 20 measurements from 100 rpm to 0.1 rpm (Supplementary Fig. S1). Each measurement is a step-lasting 30 s or until the stabilization of the torque.

The Fig. 3 shows the procedure. After the test, the rotational speed and torque values are computed and converted respectively into the shear rate and shear stress. Moreover, the shear stress τ, the shear rate $\dot{\gamma}$
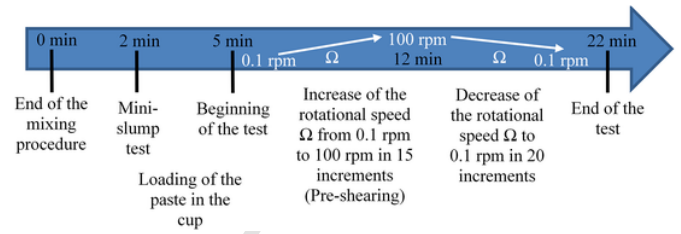

Fig. 2. 3D printed spindle into its shaft.

Fig. 3. Timeline for rheological experiments.

and the apparent viscosity μ are calculated by the following equations, where N and Γ are respectively the rotational speed and the torque:

$$\tau = K_\tau \times \Gamma \qquad (2)$$
$$\dot{\gamma} = K_\tau/K_\mu \times N \qquad (3)$$
$$\mu = K_\mu \times \Gamma/N \qquad (4)$$

Thereafter the yield stress τ_0 is estimated as the intercept of the linear regression of the curve $\tau = f(\dot{\gamma})$, where $\dot{\gamma} > 1\ s^{-1}$ (Supplementary Fig. S2), in agreement with the publication of the NIST [38]. Similarly, the plastic viscosity is defined as the slope of this curve. The dynamic yield stress and static yield stress results are available in other studies [39,67].

2.5. Mix design of the cement pastes

The mixes are gathered in Table 1. The experimental plan relies on a 2^4 full-factorial design. This allows studying the effect of each variable and of all the combinations of the variables [40]. The water/cement ratio was kept at 0.345. The amount of water added varied with the quantity of water present in the admixtures introduced to keep the total amount constant. The solid content of the admixtures is reported. The proportion of SP was inspired by the work of Zhang et al. [9], who used 0.26% of superplasticizer and the technical data sheet. The amount of X, A and VMA were chosen relying on the manufacturer recommendations. The amount of C was chosen between 0.5% and 1.3%. Quanji et al. [29] found that there is an improvement of the rheological properties, but that above 1.3%, a decrease in the yield stress is observed. Besides, 0.3% of nanoclays was used in a previous study [27]. The low value of VMA is explained by the fact that the solid content of this polymer is very low (Supplementary Table S1). Hence, 0.004% of polymers corresponded to a high quantity of liquid admixture.

Table 1
Mix design for cement pastes.

Materials (kg/m³)			Admixture (%w/w)				
Mix N°	Gub-8SF	Water	SP	X	A	C	VMA
M1	1505	508	0.26	–	–	–	–
M2	1505	502	0.26	–	–	–	0.004
M3	1505	508	0.26	–	–	0.5	–
M4	1505	502	0.26	–	–	0.5	0.004
M5	1505	496	0.26	–	0.7	–	–
M6	1505	490	0.26	–	0.7	–	0.004
M7	1505	496	0.26	–	0.7	0.5	–
M8	1505	490	0.26	–	0.7	0.5	0.004
M9	1505	497	0.26	0.3	–	–	–
M10	1505	492	0.26	0.3	–	–	0.004
M11	1505	497	0.26	0.3	–	0.5	–
M12	1505	492	0.26	0.3	–	0.5	0.004
M13	1505	486	0.26	0.3	0.7	–	–
M14	1505	480	0.26	0.3	0.7	–	0.004
M15	1505	486	0.26	0.3	0.7	0.5	–
M16	1505	480	0.26	0.3	0.7	0.5	0.004

2.6. Yield stress measurement of the mortar

Rheological tests were conducted on mortars. Since these materials are more viscous than the cement paste, the Ball Measuring System (BMS) was used. This consists of a large bowl in which an eccentric ball is put in rotation by a rotational rheometer [41]. The sphere performs one single turn in the container. In fact, cementitious materials have a shearing memory [42]. When passing through the mixture, the ball changes its structure locally, and as a result, any location where the fluid has already been sheared will not have the same behavior for further measurements [43]. The rheometer was controlled using the pre-programmed BMS template. The rotational speed was controlled with a logarithmic ramp with a shear rate $\dot{\gamma}$ ranging from 0.03162 s^{-1} to 31.62 s^{-1} and the torque was measured. The shear rate was chosen to be in the same range as the one for the cement pastes. Fischer et al. [44] showed that best results are obtained under 30 s^{-1}. The software transforms the torque into shear stress τ. Three models were fit to the data.

The Power Law model can be described by:

$$\tau = k \times \dot{\gamma}^n \tag{5}$$

where the shear stress is represented by τ and the shear rate by $\dot{\gamma}$. The parameters k and n are respectively the consistency index and the flow index. The consistency index is related to the viscosity of the fluid: the higher it is, the more viscous the fluid.

The Bingham model is expressed as:

$$\tau = \tau_0 + \mu \times \dot{\gamma} \tag{6}$$

where the shear stress and shear rate are respectively τ and $\dot{\gamma}$, while μ is the plastic viscosity. The yield stress is represented by τ_0. This model is a linear approximation of the curve.

Finally, the Herschel-Bulkley (HB) model is defined by Eq. (7):

$$\tau = \tau_0 + k \times \dot{\gamma}^n \tag{7}$$

where τ is the shear stress; $\dot{\gamma}$ is the shear rate; k is the consistency index; n is the flow index and τ_0 is the yield stress. This model allows the combined presence of a yield stress and a non-linear growth of the shear stress.

The mortars tested had exactly the same mix design as the cement pastes, but with sand. The sand/cement ratio was kept at 1.8 in this work. In their study, Le et al. [3] found two sand/binder ratios which permitted the extrudability of the mix. They preferred a 1.5 ratio to 1.8 because it allowed them to increase the amount of micro polypropylene fibers. In the present study, there are no fibers, and the 1.8 ratio is chosen to allow more sand for economics and environmental reasons. The mix design is presented in Supplementary Table S2. Additional tests were conducted on the mortar and the results are available in Charrier and Ouellet-Plamondon [45].

2.7. Analysis of results

The full-factorial design allowed us to observe all possible combinations of our admixtures, and therefore, a large panel of results. Linear regressions between the different cement paste tests were conducted to identify relationships between several experiments. The coefficient of determination and the regression equation were determined. Moreover, the impact of each admixture on each test was studied in order to allow an assessment of the best mix for 3D printing.

2.7.1. Artificial Neural Network (ANN)

The utilization of ANN provided the opportunity to predict the physical characteristics of the paste or the mortar, based on the admixture composition (Fig. 4). First, a multi-linear regression was performed. The function "fitlm" of Matlab was used to compute the coefficient of regression and their *p*-value to attest of their significance. The result of the fit allows to say if it exists a multi-linear relationship between the response (yield stress, mini-slump) and the predicators variables (the four admixtures). The case of the yield stress is presented in Supplementary Fig. S3. The multilinear fit for this response is quite good ($R^2 = 0.93$ and NRMSE = 12%). A more advanced regression with an artificial neural network was implemented with Matlab. The advantage of this technique is to be able to reuse the network for new objectives by training again the network on a new dataset [46]. A hidden layer of ten neurons was kept as proposed by default by the software. However, the tools to perform regression with a neural network on Matlab (nntool and nnstart) were not used due to their overly rigid template. Other approaches are possible to set the network and different methods of prediction were later conducted [47]. The strategy adopted was to identify a network efficient enough to predict results with future data without being over-fit. A network is "overfitted" when training is so precise that its performance on training data is excellent, but at the expense of performing poorly on unseen data. Here, the choice made was to use a Bayesian regularization backpropagation. This network training function relies on the Levenberg-Marquardt optimization to update the weight and bias values of the neurons [48]. Then, the best combination of the minimized squared error and weighted sum of squared weights was determined to get a network which generalized the experimental
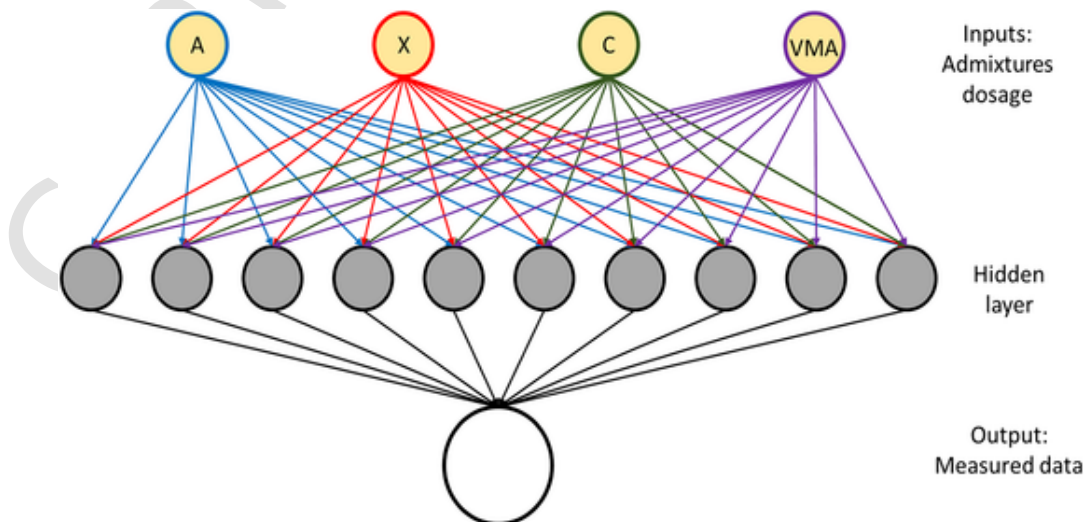

Fig. 4. Architecture of the Artificial Neural Network under study.

conditions well. In fact, adding constraints makes the network more resistant to overfitting. The Bayesian regularization has been shown to be more effective and accurate than other methods [49–52] in doing regression with artificial neural networks. The network parameters were manually modified to fit our criterion: 10 neurons in the hidden layer and a Bayesian regularization. To verify whether the model was good enough, the chosen method was to examine the Normalized Root Mean Squared Error (NRMSE). This performance indicator corresponds to the Root Mean Squared Error (RMSE) divided by the average of observation values, expressed as a percentage. The coefficients of determination R^2 were also computed to express the effectiveness of the linear relationship between the observed and predicted yield stresses.

In addition, a leave-one-out cross-validation was performed. This consisted in removing one sample of the ensemble, training the network with all the remaining data, and then testing the removed one. This operation was then repeated for every possible combination of samples. In our case, we had sixteen datasets, as a result it is a 15 combinations from a sixteen samples dataset, which can be written $\binom{16}{15} = 16$. Hence, there were sixteen different combinations of samples to train and test the model. A representation of the cross-validation method is presented in Supplementary Fig. S4. For each row of training and testing, the NRMSE and R^2 were computed. In the end, the means of each indicator was calculated to evaluate the relevance of the network. Usually, a k-fold cross-validation is performed, but in our case, the amount of data allowed us to study each possible training set. Surface responses of the values considered were then drawn from the percentage of two admixtures: one for the x-axis and one for the y-axis. The percentages of the two other admixtures were fixed. The influence of each admixture was then observed. Of the other approaches tested, the linear ANN still provided the best result to predict the yield stress, while the genetic algorithm can improve the mini-slump prediction [47].

3. Results and discussion

3.1. Viscosity of cement paste

The results of the cement paste were used to calculate viscosity, yield stress and mini-slump values for each mixture. As expected, the viscosity did not correlate with either of the other cement paste results [30,53]. The viscosity describes the capacity of the cement paste to flow. The lower the viscosity, the easier it is to pump the material. The plastic viscosity is not linearly correlated to the yield stress. Hence, minimizing the viscosity while increasing the yield stress was achievable. The VMA, which is supposed to increase the viscosity [43], has the opposite effect for mixes with SP, SP C, and SP A C (Fig. 5). The mixes showing the highest viscosity values are SP C and SP VMA C. Nanoclay has been shown to increase the viscosity in self-consolidating concrete [28]. The fact that these admixtures were often studied with self-consolidating concretes, and not with stiffer pastes, may possibly explain the different results with VMA.
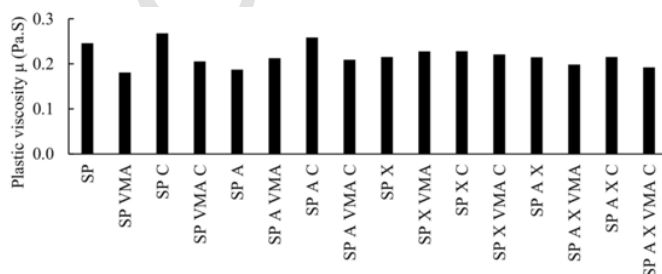
3.2. Specific Rebuilding Energy (SRE)

The thixotropic loop is widely used to measure the flocculation of cementitious materials [9,11,54]. In a classical flow curve measuring process with a rheometer, measuring an up-curve then a down curve, neither curve superimposes. Cementitious materials are sensitive to their flow history. As a result, the down curve is under the up-curve. The area between both curves has been called the Specific Rebuilding Energy (SRE). However, the value obtained cannot be considered as an intrinsic characteristic of the material [55], but rather, only represents a qualitative way of comparing several mixtures. The SRE is then a method for assessing the rebuilding capacity of a given paste. The SRE was computed in Matlab using trapezoidal numerical integration and subtracting the area under the two curves. The difference between the stiffness of the paste at rest and after a period of shearing is an important indication of the capacity of the mixture to regain stability after shearing. In 3D printing, the material shears through a nozzle before being deposited, and therefore, a high SRE is preferable because it indicates that the material has a great capacity to regain strength at rest. The SRE of each admixture is represented in Fig. 6. The mixes SP X, SP X VMA, SP X C and SP X VMA C are the four mixes with an SRE above 50. Both mixes containing VMA stand out with values of SRE exceeding 150. Finally, mixes with the accelerator generally have a lower SRE than the median value. This indicates that the presence of the accelerator tested inhibits flocculation and the ability of the paste to maintain its shape. Mixes having a high SRE are relevant for 3D printing. They testify to a potentially stiffer paste at rest and are capable of flowing easily again when sheared during the extrusion.

3.3. Yield stress and mini-slump

The yield stress τ_0 from rheological measurements and from the mini-slump test have a strong correlation with a Power law fit. This approach is also used by Tregger et al. [56], but their yield stress values are lower because they studied self-consolidating concrete (SCC) (water/binder 0.32 to 0.40 and superplasticizer content from 0.35% to 0.55%). In fact, the equation from their experimental results does not fit with this study, as the yield stress values are 10^4 times too high for our data. The equation used by Kokado & Miyagawa [57] and its modification to take into account the surface tension effect by Roussel et al. [7] (water/binder ratio from 0.4 to 0.56) do not properly fit the outcomes of this investigation as well. Their correlation equations are also for SCC. Both models are displayed alongside the experimental data and its Power law fit on the Supplementary Fig. S5. In this study, the R^2 of Eq. (8) is 0.96 and the equation is as follows:

$$\tau_0 = 54224 \times S^{-1.728} \tag{8}$$

where τ_0 is the yield stress and S is the spread of the mini-cone in %. As soon as the mini-slump drops below 160%, the discrepancy with the SCC equations is clear. The exponent of the fit of the experimental data is lower than that of the two other models. As a result, the curve is flatter for our fit, which is explained by the definition of the yield stress it-
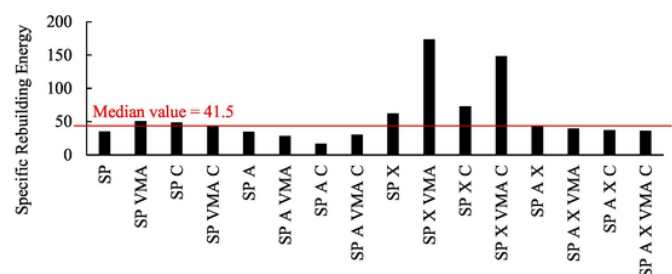

Fig. 5. Plastic viscosity for mixes 1 to 16.

Fig. 6. Specific rebuilding energy for mixes 1 to 16.

self, as there are different measurement conventions. In fact, conducting a measurement of the yield stress influences what is measured. For example, some authors use a very low shear rate [58] to conduct the experiment, while others use the up-curve/down-curve method [10]. Moreover, the model from the Roussel et al. [7] study is valid when the long-wave approximation is verified, as long as the height of the sample is at least twice as small as its radius. This approximation is valid for every sample in this study. However, some of them were not only submitted to a pure shear flow. In fact, a "hat" described by Pierre et al. [59] was observed for mixes with yield stresses above 10 Pa. This is evidence of an intermediate regime of flow. The correlation equation for this study corresponds to the SCC model when the yield stress is below 10 Pa. For 3D printing, the intermediate flow regime must be considered to predict the yield stress. The yield stress is increased with SCC models when the mini-slump is under 160%.
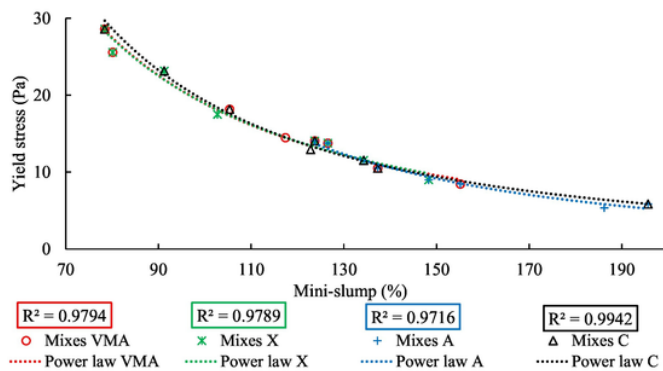

Fig. 7. Experimental data and power law fit for each admixture.

The correlation between the mini-slump and yield stress is strong for each type of admixture (Fig. 7). All admixtures lead to well-distributed values of yield stress except, for those with the accelerator, which have lower yield stresses. This admixture also had a water-reducing effect. To have a better understanding of how each admixture impacts the yield stress, the results are represented in four histograms (Fig. 8). Each histogram shows eight different mixes with and without the admixture considered. The specific actions of the VMA, the CSH seeds, the accelerator and the nanoclay are highlighted. First, the effect of the VMA (Fig. 8.a) and the X (Fig. 8.b) on the yield stress are visible for all mixes. They respectively increase it by 47% and 70% on average. The effect of the accelerator was the opposite. It enhanced the flowability of the paste because of its water-reducing effect (Fig. 8.c). Mixes with the accelerator had their yield stresses decreased by 47% on average. Finally, the nanoclay boosted the yield stress, but for some inks, the difference between some mixes with and without the admixture was very low. For example, between the mixes SP A X VMA and SP A X VMA C, the increase was only 2% (Fig. 8.d). However, on average, the increase in yield stress was 21% with the use of nanoclay.

3.4. Critical yield stress determination

The critical yield stress is the stress value that enables the fluid flow. In the context of 3D printing, after the deposition of the mixture, the critical yield stress must be high enough to allow the material to maintain its shape under its own weight. It must then increase fast enough to be able to support future layers printed above. The printed material under study is not the cement paste, but the mortar. The fit models and the observed data for mix 1 are represented in Fig. 9. For each model, the parameters are computed and the coefficient of determination R^2 is calculated to quantify the strength of the relationship between the ob-
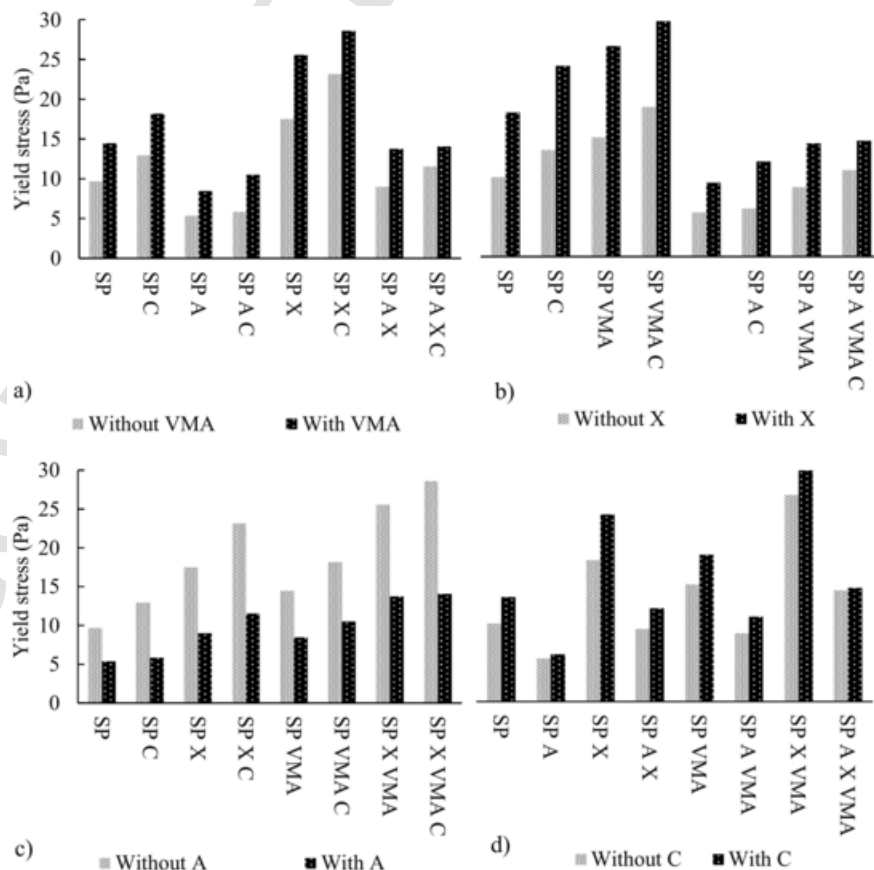

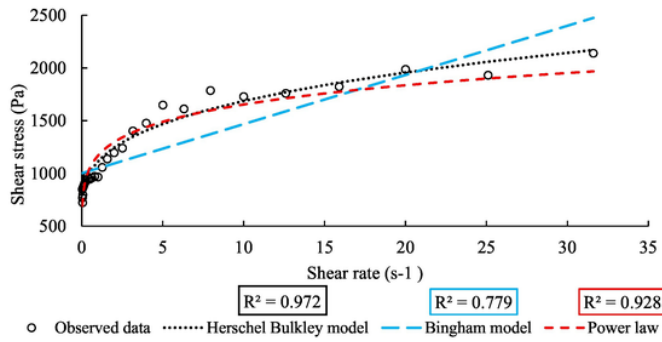Fig. 8. Effect of each admixture on the yield stress.

Fig. 9. Flow curve for mix 1 of mortar.

served shear stress and the computed one. Results are gathered in Supplementary Table S3. The yield stress for the HB model is 565 Pa, while it is 1001 Pa for the Bingham model. This discrepancy is explained by the weakness of the Bingham model in describing the non-linear part of the curve at low shear rates [20]. The coefficient of consistency and the flow index for the Power law model are twice the values for the HB model. This is explained by the fact that the Power law model does not have a term describing the yield stress. Hence, for low shear rate values, the parameters have to be higher to reach the same shear stress value. The Herschel-Bulkley model best describes the relationship between the shear stress and the shear rate. This model is widely used by researchers, and it can give better results than the Bingham model [60–62].

Four mixes were tested with the ball measuring system. The best fit is achieved with the Herschel-Bulkley model. The yield stress values obtained for the mortar with the HB model are compared to those of the respective cement pastes (Supplementary Fig. S6). A linear regression is computed. The coefficient of determination is $R^2 = 0.97$. Eq. (9) describes the regression:

$$\tau_{0,mortar} = 81.081 \times \tau_{0,cement} - 255.64 \qquad (9)$$

The results for the mortar yield stress calculated with the cement yield stress values are computed in Supplementary Table S4. The printable yield stresses proposed by Le et al. [3] goes from 300 to 900 Pa. Consequently, the values computed in this study are comparable to those from Le et al. [3] . According to Roussel [63], the initial yield stress τ_0 of a printed layer has to be higher than the critical value of ρgh_0, where ρ is the density of the paste; g is the gravity acceleration, and h_0 is the height of the printed layer. In our case, the printed material is the mortar. In the literature several dimensions of nozzles are used but Buswell et al. [64] estimate that the diameter of nozzles are commonly from 6 to 50 mm. If we take the mean of the surfaces generated by those diameters it leads to 996 mm², the square root of this value is

32 mm. Consequently, a height h_0 of 32 mm is considered in this study. For one layer, we obtain the condition $\tau_{0,mortar} > 733.5$ Pa. For the remainder of the study, the condition on the yield stress of the mortar is converted to a condition on the cement paste. From Eq. (9), we obtain the value of $\tau_{0,cement} > 12.2$ Pa. If h_0 is 50 mm, the critical yield stress is $0.050 \times g \times \rho = 1146$ *Pa* according to the expression ρgh_0 proposed by Roussel [63].

3.5. Yield stress prediction with Artificial Neural Network

In order to predict the yield stress of the cement paste from its composition in terms of admixtures, sixteen artificial neural networks were trained and tested. Each Normalized Root Mean Squared Error (NRMSE) is computed in Supplementary Table S5, with the corresponding coefficient of determination R^2. On average, the networks predict the yield stress with an error of 3.7% and the regression predictions fit the targets very well, with an average R^2 of 0.993. As a result, the implementation of an ANN to predict the yield stress with the dosage in admixtures is found to be legitimate. Network 14 is chosen for the study because its NRMSE of 1.3% and R^2 of 0.999 are respectively the lowest and the highest among all the networks.

The yield stress obtained experimentally is shown next to the one obtained with network 14 for each mixture (Fig. 10.a). The predictions match the observed values almost perfectly. Consequently, the role of each admixture is studied. To examine the evolution of yield stress as a function of the inputs, a three-dimensional analysis is carried out. First, for fixed accelerator and nanoclay dosages, four different response surfaces to the variations of CSH-seed and VMA dosages for the yield stress are represented.

The expression of the mortar yield stress by the cement paste yield stress (Eq. (9)) leads to the condition of a critical yield stress for cement paste of $\tau_{cc} = 12.2$ Pa. The maximal height of one layer for each mix can be calculated as a function of the yield stress. For example, mix 12 has a yield stress of 28.6 Pa. According to Eq. (9), h_0 is 28 mm high. In Fig. 11.a, the yield stress is shown as a function of the dosage of X and VMA, from the YZ and XZ views. The suitable admixture dosages are those with a yield stress above the critical yield stress line. The presence of X was crucial to meeting the requirement for the mixes containing 0.7% of A. In fact, below 0.23% of X, the yield stress cannot ensure the stability of an individual layer of printed mortar for mixes containing 0% of C. This value drops to 0.18% when there is 0.5% of C. In Fig. 11.b, a condition is added on the dosage in VMA. If it is greater than 0.0025% in weight of cement, the requirement is met for mixes containing 0% of C. For those with 0.5% of C, only the presence of at least 0.001% of VMA is needed. Those conditions are required to meet the yield stress requirement for mixes containing 0.7% of A.
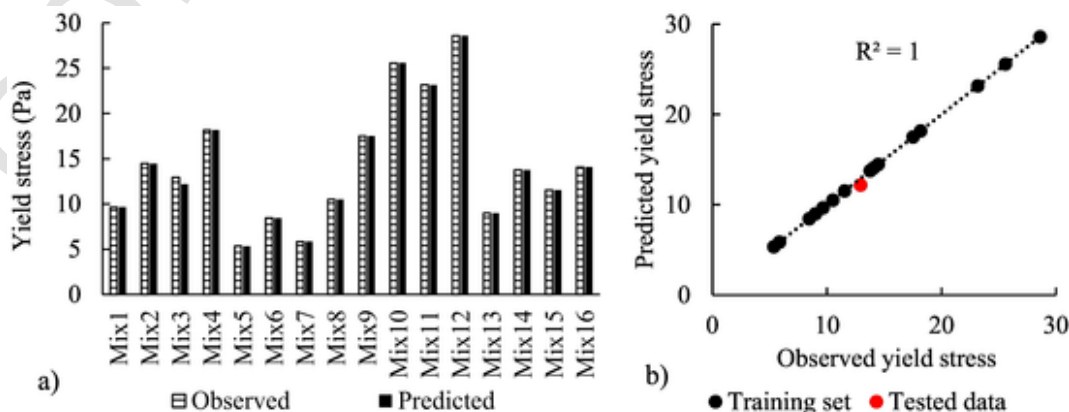

Fig. 10. a) Histogram of observed yield stress and obtained via the 14th network; b) Network predicted versus observed yield stress for mixes 1 to 16.
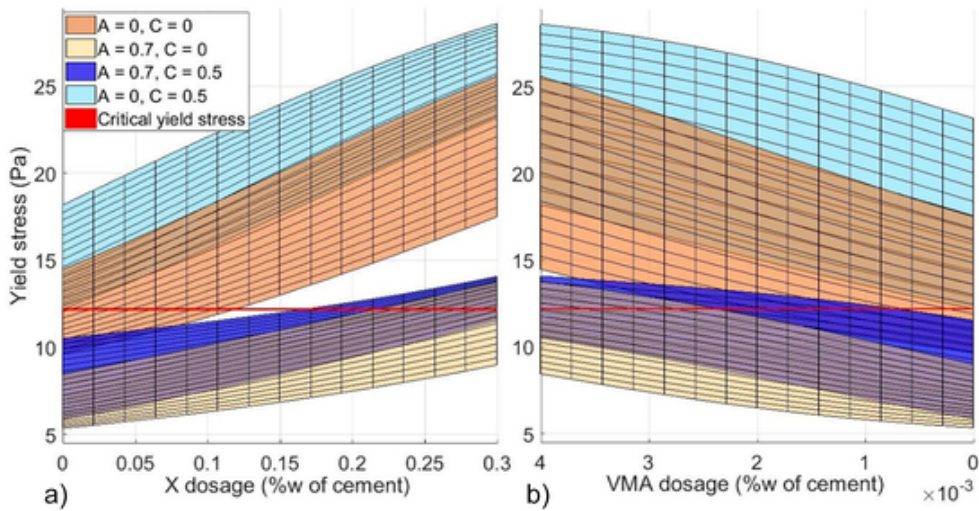
Fig. 11. Surface responses of yield stress when varying X and VMA for given values of A and C: a) View from the XZ plan; b) View from the YZ plan.

When the mixture does not involve A, the critical yield stress is easier to reach. For example, with C = 0.5% the presence of X or VMA is not required to go over 12.2 Pa. In contrast, the mix with 0% of C needs a dosage of X or VMA greater than, respectively, 0.11% and 0.0021%.

The same study was conducted for fixed values of A and VMA, while X and C dosage varied. The critical yield stress is shown as a red line in both Figs. 12.a and 12.b. First, the heights of the surfaces on the Z-axis are smaller than in Fig. 12.b. This indicates that the presence of X had a greater influence on the yield stress than did C. Once again, the mixes containing 0.7% of A are almost never eligible to 3D printing regarding the critical yield stress. The one with 0% of VMA does not meet the 12.2 Pa requirements. With 0.004% of VMA, the requirement can be achieved for a dosage in X greater than 0.16%. However, the critical yield stress is reached for a concentration in X of 0.21%. The quantity of C has almost no influence once the concentration of X has reached this value. The zone above the red line has a practically constant height (Fig. 12.b). The mixtures without this type of accelerator tend to have a higher yield stress. For the one with 0.004% of VMA, the critical yield stress is exceeded irrespective of the proportions of X or C. For the one with 0% of VMA, a proportion of X greater than 0.11% ensures a yield stress above 12.2 Pa (Fig. 12.a), while only a dosage of 0.5% of C can bring the same result (Fig. 12.b). Below this value, the mixture must include a certain amount of X to meet the required critical yield stress.

For the study with fixed values of C and VMA, the variations of X and A almost counterbalance each other (Fig. 13). No percentage of X

could ensure a yield stress greater than the requirement without considering the dosage of A. However, if there is no VMA in the mixture, reaching the critical yield stress is possible for the mix at 0% of C when two conditions are fulfilled. First, the concentration of X must be higher than 0.12% (Xmin). Secondly, the concentration of A must be lower than a value expressed as a function of the concentration of X (Eq. (10)). This equation represents the part of the surface above the critical yield stress:

$$A \leq 1.72 \times Xmin - 0.206 \qquad (10)$$

For the mix at 0.5% of C, the minimum value for X drops to 0% (Fig. 13.a) and the inequality becomes Eq. (11):

$$A \leq 2.08 \times Xmin \qquad (11)$$

Hence, the incorporation of C into the mixture allows a decrease of the concentration of X and an increase of that of A. The same comportment is observed for VMA, but the influence of this admixture is more significant. The slope of the yield stress increase is greater per amount of VMA. It can be observed that with 0% of C, a concentration of X or A respectively greater than 0.21% and lower than 0.15% ensures to meet the requirements. For 0.5% of C, these concentrations become 0.16% and 0.42%.

The analysis of the surface responses of the yield stress when setting A and X showed once again that A decreases the yield stress and X enhances it. No matter the quantity of C or VMA, when there is 0.7% of A,
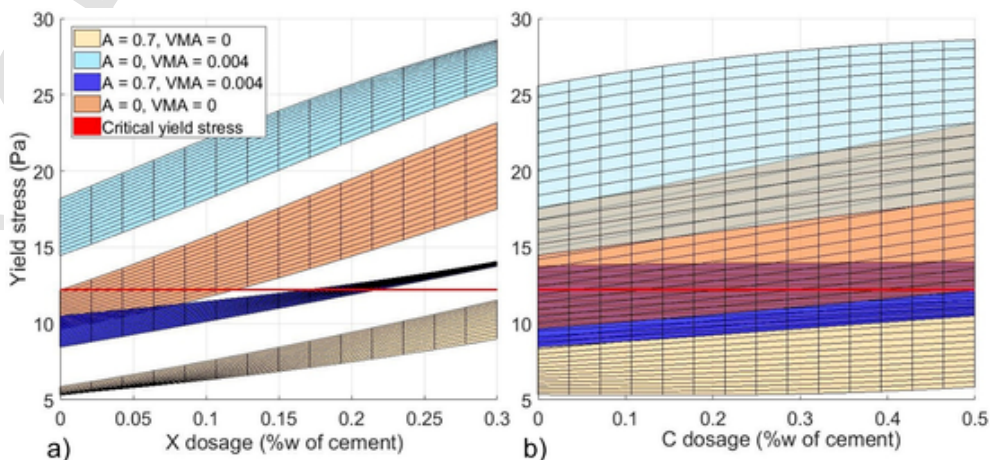

Fig. 12. Surface responses of yield stress when varying X and C for given values of A and VMA: a) View from the XZ plan; b) View from the YZ plan.
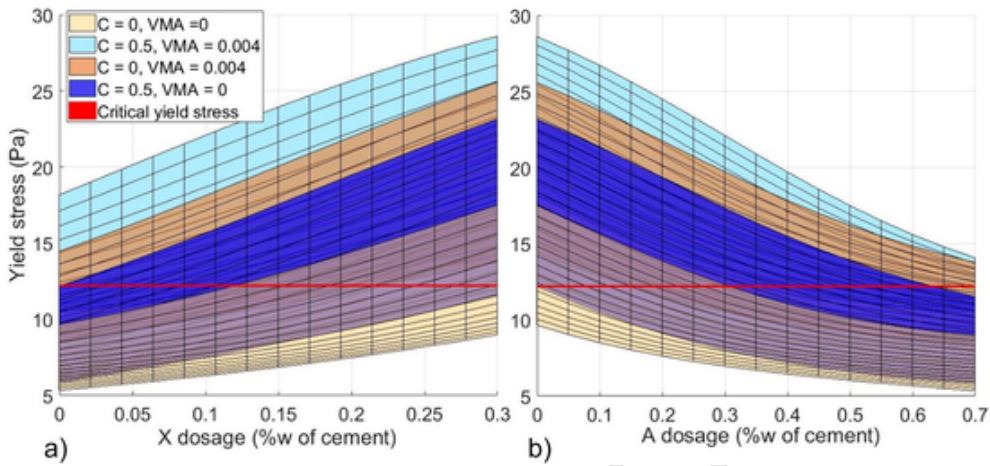
Fig. 13. Surface responses of yield stress when varying X and A for given values of C and VMA: a) View from the XZ plan; b) View from the YZ plan.

but no X in the mixture, the critical yield stress was not reached at the study time. Conversely, with a concentration of 0.3% of X without accelerator, the requirement is met (Fig. 14). Interesting results were observed for a dosage of C between 0% and 0.5% and for a dosage of VMA between 0.0015% and 0.0026%. In this zone, the surfaces corresponding to the mixtures A = 0%, X = 0% and A = 0.7%, X = 0.3% merge (Fig. 14.a). Moreover, for low values of C or VMA, the surfaces are almost superimposed. This means that the effects of A and X compensate each other, at least when the quantities of the two other admixtures are low. In fact, when both concentrations of C and VMA increase, the mixture without A and X gains more in yield stress than does the one with both admixtures.

The study of the variations of the yield stress when setting C and A showed approximately the same behavior as when setting X and A. We see in Fig. 15.a that the variations of C had almost no influence on the yield stress, while A showed a decrease in yield stress when increasing. One mix can again does not meet the printing requirements, the absence of X and VMA leads to a yield stress too low (Fig. 15).
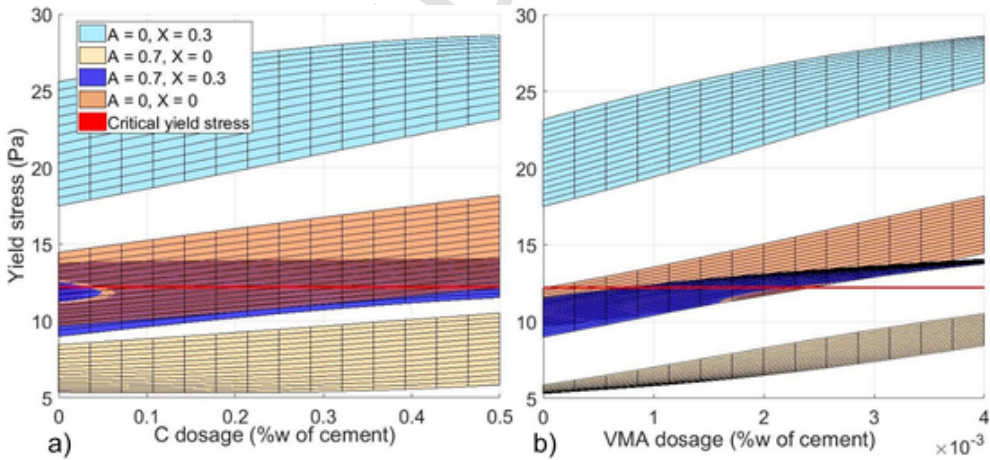

Fig. 14. Surface responses of yield stress when varying C and VMA for given values of A and X: a) View from the XZ plan; b) View from the YZ plan.
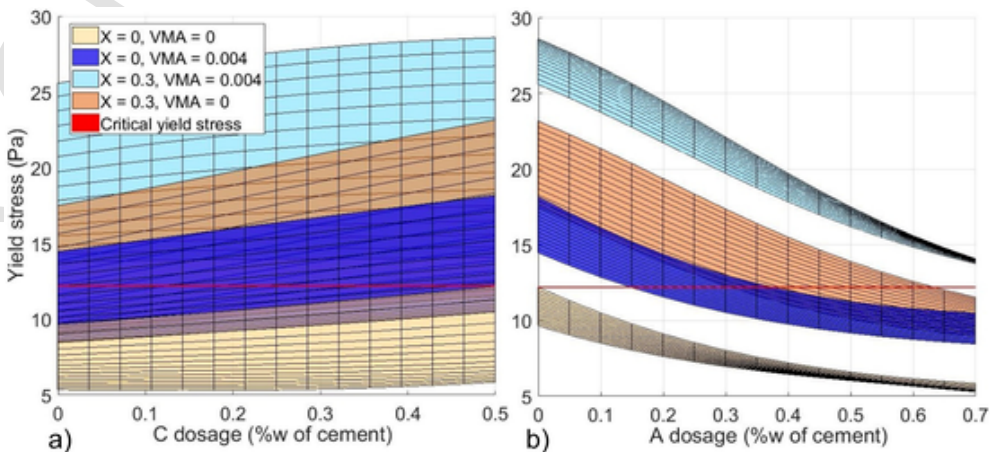

Fig. 15. Surface responses of yield stress when varying C and A for given values of X and VMA: a) View from the XZ plan; b) View from the YZ plan.

Finally, setting X and C while varying VMA and A leads to the same representation as in the previous composition. The increase in the yield stress with the VMA was greater than for the C (Fig. 16.a). Every surface overlapped on the following one. This means that the critical yield stress was reached no matter the mixture if the concentrations of VMA and A were adjusted.

The study of the influence of each admixture on the yield stress allows drawing several conclusions. Firstly, the accelerator A has a water reducer effect, which drastically decreases the yield stress. In fact, a concentration of 0.7% without any other admixture leads consistently to a paste with a yield stress below the critical value. Nevertheless, accelerators are widely used in 3D printing in order to reach a compressive strength sufficient to face the weight of several layers of material [3,27,64–66]. That is why the incorporation of other admixtures, such as the X, the C or the VMA, is important with this A. A comparison between these last three highlights the fact that the X is the most effective. The shapes of the surfaces (Figs. 13.a, 16.a, and 15.a) show a greater slope for the increase of X, followed by VMA and, last, C. However, the proportion of VMA was between 0 and 0.004%, while the X varied between 0 and 0.3%. In view of the mass proportions of each admixture, the VMA appeared more effective than the X. Moreover, the C is less effective than the X for increasing the yield stress, despite a higher percentage of addition. Hence, more X can substitute the incorporation of C. The C still improves the correlation between the yield stress and the mini-slump tests [45]. Finally, the X is a solution to counterbalance the water-reducing effect of A, because the mixtures containing neither or both of them almost give the same yield stress.

3.6. Mini-slump prediction with ANN

The same procedure was conducted with the mini-slump results. The average NRMSE was 6.5% and the average coefficient of determination R^2 was 0.94. The NRMSE and R^2 for all the networks are listed in Supplementary Table S6. The best values of the indicators are found for network 13, with $R^2 = 0.96$ and NRMSE = 0.054. The mini-slump observed and calculated with the network 13 is shown in Fig. 17.a. The linear regression between the observed values and the predicted ones are computed in Fig. 17.b. The network was suitable to describe the mini-slump. Other predictions with the mini-slump results are available in Sergis et al. [47].

To observe the evolution of the mini-slump as a function of the different admixtures, six three-dimensional analyses were conducted. Graphics are shown in Fig. 18. The outcome of this study agrees with the previous result on the correlation between yield stress and mini-slump: an increase in yield stress corresponds to a decrease in the mini-slump value. Consequently, the admixtures X, VMA and C tend to decrease the mini-slump. X has a greater influence than does VMA and C on the decrease. The incorporation of A leads to higher mini-slump values. There is almost no difference between a mix with 0.7% of A and 0.3% of X and a mix with no A and X (Fig. 18.f). Following Eq. (8), a critical yield stress of 12.2 Pa for cement paste corresponds to a mini slump of 129%. As a result, every part of a mini-slump response surface which is above this value should be considered as not suitable for printing, while those below are suitable (Fig. 18).
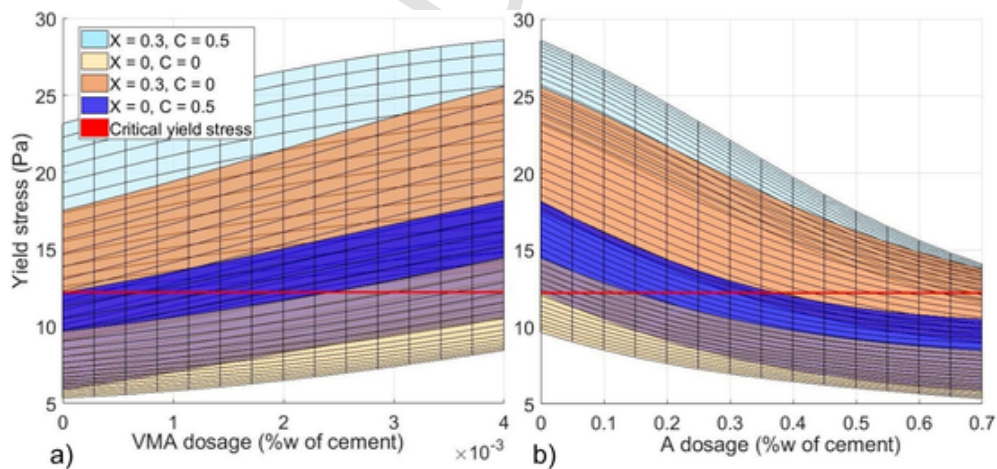

Fig. 16. Surface responses of yield stress when varying VMA and A for given values of X and C: a) View from the XZ plan; b) View from the YZ plan.
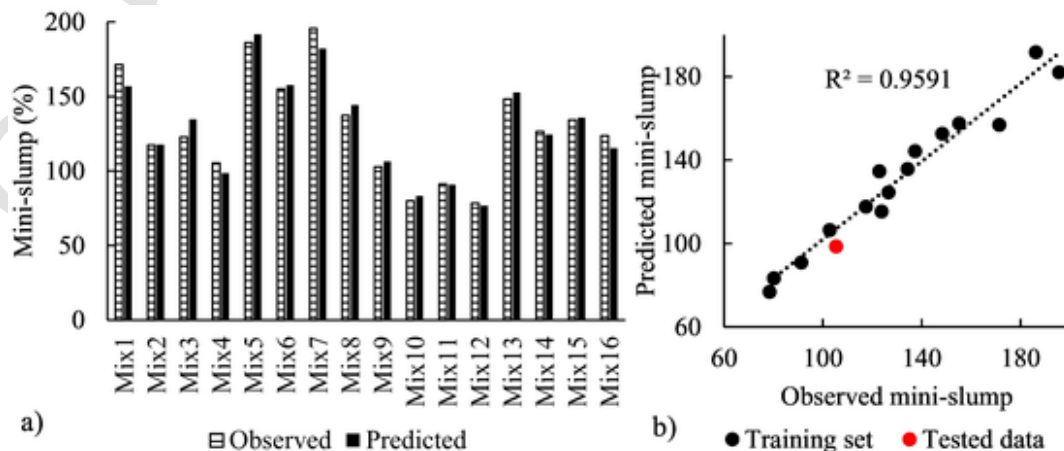

Fig. 17. a) Histogram of observed mini-slump and that obtained via the 13th network; b) Network predicted versus observed mini-slump for mixes 1 to 16.
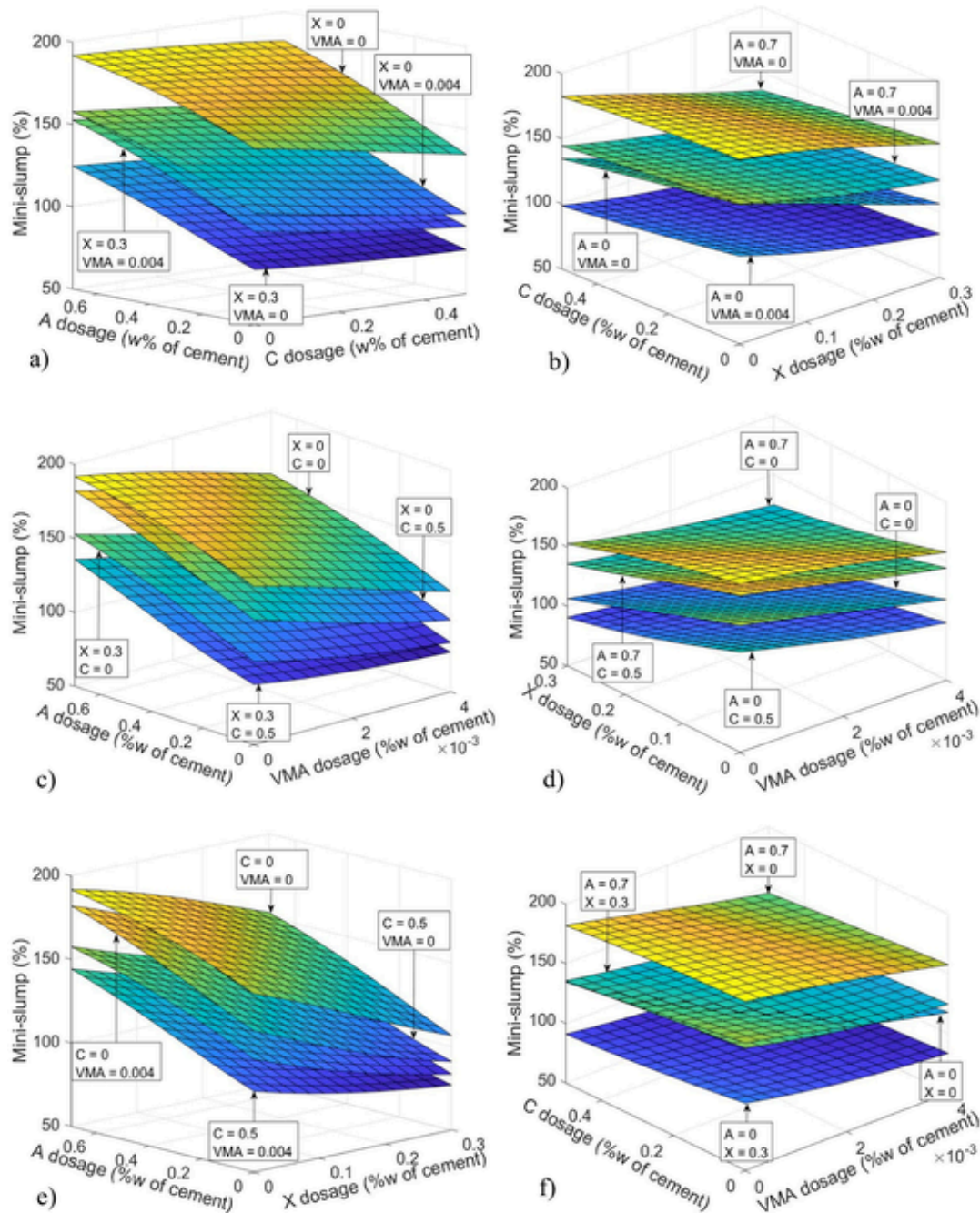
Fig. 18. Mini-slump as a function of a) A and C with fixed X and VMA b) X and C with fixed A and VMA; c) A and VMA with fixed X and C; d) X and VMA with fixed A and C; e) A and X with fixed C and VMA; f) VMA and C with fixed A and X.

3.7. Simulation of new mixes and correlation between the neural networks

In order to verify the robustness of our neural network, 256 new mixes were generated with values between the bounds of admixtures. Those 256 new mixes were then entered into both the mini-slump and the yield stress networks. The results of the mini-slump network were calculated as yield stress values with Eq. (8). Supplementary Fig. S7 explains the simulation procedure. Finally, a linear regression was performed to confirm the effectiveness of the ANN, as shown in Fig. 19. The R^2 value is 0.98, and the simulation confirms the effectiveness of the ANNs.
the yield stress networks. The results of the mini-slump network were calculated as yield stress values with Eq. (8). Fig. S7 demonstrates the simulation procedure. Finally, a linear regression was performed to

confirm the effectiveness of the ANN, as shown in Fig. 19. The R^2 value is 0.9857, and the simulation confirms the effectiveness of the ANNs.

4. Conclusions

In this article, several cement pastes containing superplasticizer, accelerator, viscosity modifying agent, nanoclays and CSH seeds were studied. The mini-slump test, considered easy to implement, was conducted on each paste. A rheometer was also used to identify the rheological properties of the pastes. The mini-slump correlated well with the dynamic yield stress τ_0 using a Power law. Conversely, the viscosity and the SRE had no significant correlation with the yield stress.

The role of each admixture in the behavior of the paste was investigated. The mini-slump and the yield stress results agreed for every type
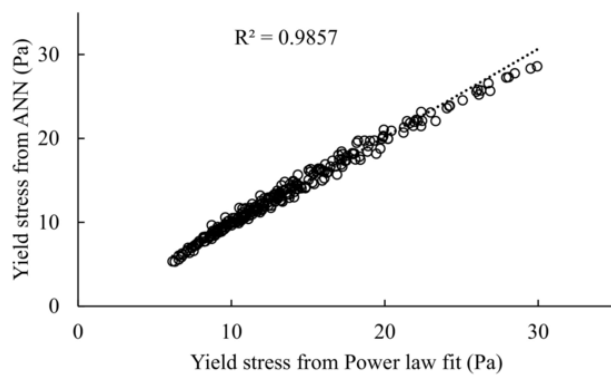
Fig. 19. Correlation between yield stress from ANN (based on rheometer measurements) and from Power law fit with mini-slump.

of admixture. Furthermore, their influence on the yield stress was highlighted, showing that X, VMA and C tend to increase τ_0, while this specific A tends to decrease it. Another type of accelerator can be tested at a later stage.

The critical yield stress was identified with a 32 mm high layer of printed material. The criterion on the yield stress to ensure printability implies that if it is required to print a thicker layer, the critical yield stress must be higher. The criterion was defined for mortar and adapted for cement paste.

An artificial neural network was successfully trained to be able to predict the yield stress as a function of the percentage in weight of cement of each admixture. Once represented, the surface responses provided information about the global influence of each admixture. Moreover, by drawing the surface corresponding to the critical yield stress in red, the specific critical percentage was identified, when comparing the views from the XZ and YZ plans. The same work was conducted for the mini-slump.

Finally, the simulation of 256 other random mixes allowed obtaining 256 yield stress and 256 mini-slump values with ANNs. The 256 mini-slump values are transformed into other yield stress values by the Power law relating yield stress and mini-slump. A linear regression between the yield stresses from the ANN and from the Power law confirms the robustness of the neural networks. Consequently, artificial neural networks can predict the fresh properties of cementitious materials according to different admixtures. Future work can involve a time factor in the ANN to describe the evolution of the yield stress during printing. The result would allow to predict the cementitious material printability over time.

Credit authorship contribution statement

The authors confirm contributions to the paper as follows: study conception and design: C.M.O.P. and M.C.; data collection: M.C.; analysis and interpretation of results: M.C. and C.M.O.P.; draft manuscript preparation: M.C. and C.M.O.P. Both authors reviewed the manuscript.

Uncited reference

Declaration of competing interest

All persons who meet authorship criteria are listed as authors, and all authors certify that they have participated sufficiently in the work to take public responsibility for the content, including participation in the concept, design, analysis, writing, or revision of the manuscript. Furthermore, each author certifies that this material or similar material has not been and will not be submitted to or published in any other publication.

Acknowledgement

Appendix A. Supplementary data

Supplementary data to this article can be found online at https://doi.org/10.1016/j.cemconres.2022.106761.

References

[1] E. Lloret, A.R. Shahab, M. Linus, R.J. Flatt, F. Gramazio, M. Kohler, S. Langenberg, Complex concrete structures: merging existing casting techniques with digital fabrication, Comput. Aided Des. 60 (2015) 40–49.

[2] C. Gosselin, R. Duballet, P. Roux, N. Gaudillière, J. Dirrenberger, P. Morel, Large-scale 3D printing of ultra-high performance concrete – a new processing route for architects and builders, Mater. Des. 100 (2016) 102–109.

[3] T.T. Le, S.A. Austin, S. Lim, R.A. Buswell, A.G.F. Gibb, T. Thorpe, Mix design and fresh properties for high-performance printing concrete, Mater. Struct. 45 (2012) 1221–1232.

[4] A. Bouvet, E. Ghorbel, R. Bennacer, The mini-conical slump flow test: analysis and numerical study, Cem. Concr. Res. 40 (2010) 1517–1523.

[5] J. Gao, A. Fourie, Spread is better: an investigation of the mini-slump test, Miner. Eng. 71 (2015) 120–132.

[6] Z. Tan, S.A. Bernal, J.L. Provis, Reproducible mini-slump test procedure for measuring the yield stress of cementitious pastes, Mater. Struct. 50 (2017) 235.

[7] N. Roussel, C. Stefani, R. Leroy, From mini-cone test to abrams cone test: measurement of cement-based materials yield stress using slump tests, Cem. Concr. Res. 35 (2005) 817–822.

[8] P. Yang, S.A.O. Nair, N. Neithalath, in: Discrete Element Simulations of Rheological Response of Cementitious Binders as Applied to 3D Printing, 2019, pp. 102–112.

[9] Y. Zhang, Y. Zhang, G. Liu, Y. Yang, M. Wu, B. Pang, Fresh properties of a novel 3D printing concrete ink, Constr. Build. Mater. 174 (2018) 263–271.

[10] A. Olivas, M. Helsel, N. Martys, C. Ferraris, W. George, R. Ferron, Rheological measurement of suspensions without slippage: experiment and model, in: D.O. Commerce (Ed.), NIST Technical Note 1946, 2016.

[11] S. Kawashima, J.H. Kim, D.J. Corr, S.P. Shah, Study of the mechanisms underlying the fresh-state response of cementitious materials modified with nanoclays, Constr. Build. Mater. 36 (2012) 749–757.

[12] Y. Qian, S. Kawashima, Distinguishing dynamic and static yield stress of fresh cement mortars through thixotropy, Cem. Concr. Compos. 86 (2018) 288–296.

[13] J.E. Wallevik, Relationship between the bingham parameters and slump, Cem. Concr. Res. 36 (2006) 1214–1221.

[14] H. Van Damme, Concrete material science: past, present, and future innovations, Cem. Concr. Res. 112 (2018) 5–24.

[15] M.A. DeRousseau, J.R. Kasprzyk, W.V. Srubar, Computational design optimization of concrete mixtures: a review, Cem. Concr. Res. 109 (2018) 42–53.

[16] N.R. Washburn, A. Menon, C.M. Childs, B. Poczos, K.E. Kurtis, Machine learning approaches to admixture design for clay-based cements, in: F. Martirena, A. Favier, K. Scrivener (Eds.), Calcined Clays for Sustainable Concrete, Springer, Netherlands, Dordrecht, 2018, pp. 488–493.

[17] A. Menon, C. Gupta, K. Perkins, B.L. DeCost, N. Budwal, R.T. Rios, K. Zhang, B. Poczos, N.R. Washburn, Elucidating Multi-physics Interactions in Suspensions for the Design of Polymeric Dispersants: A Hierarchical Machine Learning Approach, 2017.

[18] D. Marchon, S. Kawashima, H. Bessaies-Bey, S. Mantellato, S. Ng, Hydration and rheology control of concrete for digital fabrication: potential admixtures and cement chemistry, Cem. Concr. Res. 112 (2018) 96–110.

[19] M. Toledano-Prados, M. Lorenzo-Pesqueira, B. González-Fonteboa, S. Seara-Paz, Effect of polycarboxylate superplasticizers on large amounts of fly ash cements, Constr. Build. Mater. 48 (2013) 628–635.

[20] Y. He, X. Zhang, Y. Kong, X. Wang, L. Shui, H. Wang, Influence of polycarboxylate superplasticizer on rheological behavior in cement paste, journal of Wuhan University of Technology-materSci. Ed. 33 (2018) 932–937.

[21] Y. He, X. Zhang, R.D. Hooton, Effects of organosilane-modified polycarboxylate superplasticizer on the fluidity and hydration properties of cement paste, Constr. Build. Mater. 132 (2017) 112–123.

[22] M. Lachemi, K.M.A. Hossain, V. Lambros, P.C. Nkinamubanzi, N. Bouzoubaâ, Performance of new viscosity modifying admixtures in enhancing the rheological properties of cement paste, Cem. Concr. Res. 34 (2004) 185–193.

[23] P.C. Aïtcin, in: 19 - Accelerators, Science and Technology of Concrete Admixtures, Woodhead Publishing, 2016, pp. 405–413.

[24] J.J. Thomas, H.M. Jennings, J.J. Chen, Influence of nucleation seeding on the hydration mechanisms of tricalcium silicate and cement, J. Phys. Chem. C 113 (2009) 4327–4334.

[25] L. Nicoleau, New calcium silicate hydrate network, Transp. Res. Rec. 2142 (2010) 42–51.

[26] L. Reiter, T. Wangler, N. Roussel, R.J. Flatt, The role of early age structural build-up in digital fabrication with concrete, Cem. Concr. Res. 112 (2018) 86–95.

[27] A. Kazemian, X. Yuan, E. Cochran, B. Khoshnevis, Cementitious materials for construction-scale 3D printing: laboratory testing of fresh printing mixture, Constr. Build. Mater. 145 (2017) 639–647.

[28] M.A. Mirgozar Langaroudi, Y. Mohammadi, Effect of nano-clay on workability, mechanical, and durability properties of self-consolidating concrete containing mineral admixtures, Constr. Build. Mater. 191 (2018) 619–634.

[29] Z. Quanji, G.R. Lomboy, K. Wang, Influence of nano-sized highly purified magnesium alumino silicate clay on thixotropic behavior of fresh cement pastes, Constr. Build. Mater. 69 (2014) 295–300.

[30] C. Ferraris, N. Martys, Relating fresh concrete viscosity measurements from different rheometers, J. Res. Natl. Inst. Stand. Technol. 108 (2003) 229–234.

[31] G. Sant, C.F. Ferraris, J. Weiss, Rheological properties of cement pastes: a discussion of structure formation and mechanical property development, Cem. Concr. Res. 38 (2008) 1286–1296.

[32] ASTMC494, in: Standard Specification for Chemical Admixtures for Concrete, Uniformity and Equivalence Testes, ASTM International, 2017, p. 10.

[33] ASTMC1738, in: Standard Practice for High-Shear Mixing of Hydraulic Cement Pastes, ASTM International, 2014, p. 3.

[34] C. Ferraris, K. Obla, R. Hill, The influence of mineral admixtures on the rheology of cement paste and concrete, Cem. Concr. Res. 31 (2001) 245–255.

[35] D. Kantro, Influence of water-reducing admixtures on properties of cement paste - a miniature slump, TEST 2 (2) (1980) 1–8.

[36] ASTM International, Standard Test Method for Flow of Hydraulic Cement Mortar, Norme ASTM C1437, 2015.

[37] A. Olivas, C. Ferraris, W. Guthrie, B. Toman, Bingham Paste Mixture for Rheological Measurements, Special Publication 260-182, National Institute of Standard and Technology, 2015.

[38] A. Olivas, C. Ferraris, N. Martys, E. Garboczi, B. Toman, in: D.O. Commerce (Ed.), Certification of SRM 2493:Standard Reference Mortar for Rheological Measurements, National Institute of Standard and Technology, 2017, p. 192.

[39] K. Zongo, M. Charrier, C.M. Ouellet-Plamondon, C.D. C., F.L.S. Bos, Dynamic and static yield stress determination of cementitious paste with admixtures, in: R. Wolfs, T. Salet (Eds.), Second RILEM International Conference on Concrete and Digital Fabrication, Springer, Cham, 2020, pp. 370–378.

[40] J. Antony, 6 - full factorial designs, in: J. Antony (Ed.), Design of Experiments for Engineers and Scientists (Second Edition), Elsevier, Oxford, 2003, pp. 63–85.

[41] M. Schatzmann, G.R. Bezzola, H.E. Minor, E. Windhab, P. Fischer, Rheometry for Large-particulated Fluids: Analysis of the Ball Measuring System and Comparison to Debris Flow Rheometry, 2009.

[42] N. Roussel, G. Ovarlez, S. Garrault, C. Brumaud, The origins of thixotropy of fresh cement pastes, Cem. Concr. Res. 42 (2012) 148–157.

[43] A. Leemann, F. Winnefeld, The effect of viscosity modifying agents on mortar and concrete, Cem. Concr. Compos. 29 (2007) 341–349.

[44] P. Fischer, M. Schatzmann, G.-R. Bezzola, H.E. Minor, The Ball Measuring System - A New Method to Determine Debris-flow Rheology? 2003.

[45] M. Charrier, C. Ouellet-Plamondon, Testing procedures on materials to formulate the ink for 3D printing, Transp. Res. Rec. 2674 (2020) 21–32.

[46] M. Derousseau, J. Kasprzyk, W., Srubar iii, computational design optimization of concrete mixtures: a review, Cem. Concr. Res. 109 (2018) 42–53.

[47] V. Sergis, M. Charrier, C.M. Ouellet-Plamondon, Prediction of the yield stress of printing mortar ink, in: B. F (Ed.), Second RILEM International Conference on Concrete and Digital Fabrication DC 2020, Springer Eindhoven, The Netherlands, 2020, pp. 360–369.

[48] MathWorks, Documentation MathWorks : trainbr, 2019.

[49] D.S.S.H. Kaur, Bayesian regularization based neural network tool for software effort estimation, Global Journal of Computer Science and Technology 13 (2–D) (2013), Global Journal of Computer Science and Technology, (2013).

[50] F. Burden, D. Winkler, Bayesian Regularization of Neural Networks, 2009.

[51] J. Shi, Y. Zhu, F. Khan, G. Chen, Application of bayesian regularization artificial neural network in explosion risk analysis of fixed offshore platform, J. Loss Prev. Process Ind. 57 (2019) 131–141.

[52] M. Rakhshkhorshid, S.-A. Teimouri Sendesi, Bayesian regularization neural networks for prediction of austenite formation temperatures (Ac1 and Ac3), J. Iron Steel Res. Int. 21 (2014) 246–251.

[53] C. Ferraris, F. DeLarrard, Testing and Modelling of Fresh Concrete Rheology, National Institute of Standard and Technology, 1998.

[54] R. Ferron, A. Gregori, Z. Sun, S. Shah, Rheological Method to Evaluate Structural Buildup in Self-consolidating Concrete Cement Pastes, 2007.

[55] N. Roussel, A Thixotropy Model for Fresh Fluid Concretes: Theory, Validation and Applications, 2006.

[56] N. Tregger, L. Ferrara, S. Shah, Identifying viscosity of cement paste from mini-slump-flow test, Mater. J. 105 (2008).

[57] T. Kokado, T. Miyagawa, Study on a method of obtaining rheological coefficients of high-flow concrete from slump flow test, Doboku Gakkai Ronbunshu 1999 (1999) 113–129.

[58] A. Perrot, T. Lecompte, H. Khelifi, C. Brumaud, J. Hot, N. Roussel, Yield stress and bleeding of fresh cement pastes, Cem. Concr. Res. 42 (2012) 937–944.

[59] A. Pierre, C. Lanos, P. Estellé, Extension of Spread-slump Formulae for Yield Stress Evaluation, 2013.

[60] P. Banfill, Rheology of Fresh Cement and Concrete, 2006.

[61] C. Ferraris, Measurement of the rheological properties of high performance concrete: state of the art report, J. Res. Natl. Inst. Stand. Technol. 104 (1999) 461–478.

[62] D. Feys, R. Cepuritis, S. Jacobsen, K. Lesage, E. Secrieru, A. Yahia, Measuring rheological properties of cement paste: Most common techniques, procedures and challenges, RILEM Tech. Lett. 2 (2017) 129–135.

[63] N. Roussel, Rheological requirements for printable concretes, Cem. Concr. Res. 112 (2018) 76–85.

[64] R.A. Buswell, W.R. Leal de Silva, S.Z. Jones, J. Dirrenberger, 3D printing using concrete extrusion: a roadmap for research, Cem. Concr. Res. 112 (2018) 37–49.

[65] T.T. Le, S.A. Austin, S. Lim, R.A. Buswell, R. Law, A.G.F. Gibb, T. Thorpe, Hardened properties of high-performance printing concrete, Cem. Concr. Res. 42 (2012) 558–566.

[66] B. Panda, S.C. Paul, N.A.N. Mohamed, Y.W.D. Tay, M.J. Tan, Measurement of tensile bond strength of 3D printed geopolymer mortar, Measurement 113 (2018) 108–116.

[67] C. Bhojaraju, M. Charrier, C.M. Ouellet-Plamondon, How Admixtures Affect Yield Stresses of Cement, ACI Materials Journal 118 (6) (2021) 311–324, https://doi.org/10.14359/51734149.